Research Article | Vol. 24, No. 14 | 11 Jul 2016 | OPTICS EXPRESS 15383

Optics EXPRESS

Vector light shift averaging in paraffin-coated alkali vapor cells

ELENA ZHIVUN,[1] ARNE WICKENBROCK,[2,*] JULIA SUDYKA,[3] BRIAN PATTON,[1,4] SZYMON PUSTELNY,[3] AND DMITRY BUDKER[1,2,5,6]

[1]*Department of Physics, University of California, Berkeley, California 94720-7300, USA*
[2]*Johannes Gutenberg-University Mainz, 55128 Mainz, Germany*
[3]*Marian Smoluchowski Institute of Physics, Łojasiewicza 11, 30-348 Kraków, Poland*
[4]*Physik-Department, Technische Universität München, 85748 Garching, Germany*
[5]*Helmholtz Institut Mainz, 55099 Mainz, Germany*
[6]*Nuclear Science Division, Lawrence Berkeley National Laboratory, Berkeley, CA 94720, USA*
*wickenbr@uni-mainz.de

Abstract: Light shifts are an important source of noise and systematics in optically pumped magnetometers. We demonstrate that the long spin-coherence time in paraffin-coated cells leads to spatial averaging of the vector light shift over the entire cell volume. This renders the averaged vector light shift independent, under certain approximations, of the light-intensity distribution within the sensor cell. Importantly, the demonstrated averaging mechanism can be extended to other spatially varying phenomena in anti-relaxation-coated cells with long coherence times.

OCIS codes: (000.2190) Experimental physics; (020.0020) Atomic and molecular physics.

References and links

1. M. Arditi and T. R. Carver, "Pressure, light, and temperature shifts in optical detection of 0-0 hyperfine resonance of alkali metals," Phys. Rev. **124**, 800–809 (1961).
2. B. S. Mathur, H. Tang, and W. Happer, "Light shifts in the alkali atoms," Phys. Rev. **171**, 11–19 (1968).
3. M. Arditi and J. L. Picque, "Precision measurements of light shifts induced by a narrow-band GaAs laser in the 0-0 133 Cs hyperfine transition," J. Phys. B **8**(14), L331 (1975).
4. Y. Yano, W. Gao, S. Goka, and M. Kajita, "Theoretical and experimental investigation of the light shift in Ramsey coherent population trapping," Phys. Rev. A **90**, 013826 (2014).
5. E. Breschi, G. Kazakov, C. Schori, G. Di Domenico, G. Mileti, A. Litvinov, and B. Matisov, "Light effects in the atomic-motion-induced Ramsey narrowing of dark resonances in wall-coated cells," Phys. Rev. A **82**, 063810 (2010).
6. A. Brillet, "Evaluation of the light shifts in an optically pumped cesium beam frequency standard," Metrologia **17**(4), 147–150 (1981).
7. S. Ohshima, Y. Nakadan, T. Ikegami, and Y. Koga, "Light shifts in an optically pumped Cs beam frequency standard," IEEE Trans. Instrum. Meas. **40**(6), 1003–1007 (1991).
8. D. Budker, L. Hollberg, D. F. Kimball, J. Kitching, S. Pustelny, and V. V. Yashchuk, "Microwave transitions and nonlinear magneto-optical rotation in anti-relaxation-coated cells," Phys. Rev. A **71**, 012903 (2005).
9. I. A. Sulai, R. Wyllie, M. Kauer, G. S. Smetana, R. T. Wakai, and T. G. Walker, "Diffusive suppression of AC-Stark shifts in atomic magnetometers," Opt. Lett. **38**(6), 974–976 (2013).
10. A. Podvyaznyi, A. Sakantsev, and V. Semenov, "About the Zeeman light-induced frequency shift of the radio-optical resonance in optically oriented isotopes of alkali metals," Russ. Phys. J. **46**, 933 (2003).
11. J. C. Camparo, R. P. Frueholz, and C. H. Volk, "Inhomogeneous light shift in alkali-metal atoms," Phys. Rev. A **27**, 1914–1924 (1983).
12. J. Skalla, S. Lang, and G. Wackerle, "Magnetic-resonance line-shapes in optical-pumping and light-shift experiments in alkali atomic vapors," J. Opt. Soc. Am. B **12**(5), 772–781 (1995).
13. B. Bulos, A. Marshall, and W. Happer, "Light shifts due to real transitions in optically pumped alkali atoms," Phys. Rev. A **4**(1), 51–59 (1971).
14. C. Cohen-Tannoudji and J. Dupont-Roc, "Experimental study of Zeeman light shifts in weak magnetic fields," Phys. Rev. A **5**, 968–984 (1972).
15. J. M. Higbie, E. Corsini, and D. Budker, "Robust, high-speed, all-optical atomic magnetometer," Rev. Sci. Instrum. **77**(11), 113106 (2006).
16. V. Acosta, M. P. Ledbetter, S. M. Rochester, D. Budker, D. F. Jackson Kimball, D. C. Hovde, W. Gawlik, S. Pustelny, J. Zachorowski, and V. V. Yashchuk, "Nonlinear magneto-optical rotation with frequency-modulated light in the geophysical field range," Phys. Rev. A **73**, 053404 (2006).

#264741 http://dx.doi.org/10.1364/OE.24.015383
Journal © 2016 Received 9 May 2016; revised 8 Jun 2016; accepted 10 Jun 2016; published 29 Jun 2016

Optics EXPRESS

17. B. Patton, O. O. Versolato, D. C. Hovde, E. Corsini, J. M. Higbie, and D. Budker, "A remotely interrogated all-optical âĂL'87Rb magnetometer," Appl. Phys. Lett. **101**(8), 083502 (2012).
18. S. Groeger, G. Bison, J.-L. Schenker, R. Wynands, and A. Weis, "A high-sensitivity laser-pumped Mx magnetometer," Eur. Phys. J. D **38**(2), 239–247 (2006).
19. Z. GrujiÄĞ, P. Koss, G. Bison, and A. Weis, "A sensitive and accurate atomic magnetometer based on free spin precession," Eur. Phys. J. D **69**(5), 135 (2015).
20. S. J. Seltzer, P. J. Meares, and M. V. Romalis, "Synchronous optical pumping of quantum revival beats for atomic magnetometry," Phys. Rev. A **75**, 051407 (2007).
21. V. G. Lucivero, P. Anielski, W. Gawlik, and M. W. Mitchell, "Shot-noise-limited magnetometer with sub-picotesla sensitivity at room temperature," Rev. Sci. Instrum. **85**(11), 113108 (2014).
22. S. Pustelny, A. Wojciechowski, M. Gring, M. Kotyrba, J. Zachorowski, and W. Gawlik, "Magnetometry based on nonlinear magneto-optical rotation with amplitude-modulated light," J. Appl. Phys. **103**(6), 063108 (2008).
23. M. V. Balabas, T. Karaulanov, M. P. Ledbetter, and D. Budker, "Polarized alkali-metal vapor with minute-long transverse spin-relaxation time," Phys. Rev. Lett. **105**(7), 070801 (2010).
24. S. Pustelny, D. F. Jackson Kimball, S. M. Rochester, V. V. Yashchuk, and D. Budker, "Influence of magnetic-field inhomogeneity on nonlinear magneto-optical resonances," Phys. Rev. A **74**, 063406 (2006).
25. W. E. Bell and A. L. Bloom, "Optical detection of magnetic resonance in alkali metal vapor," Phys. Rev. **107**, 1559–1565 (1957).
26. Dmitry Budker and D. F. J. Kimball eds., *Optical Magnetometry* (Cambridge University, 2013).
27. F. Le Kien, P. Schneeweiss, and A. Rauschenbeutel, "Dynamical polarizability of atoms in arbitrary light fields: general theory and application to cesium," Eur. Phys. J. D **67**(5), 92 (2013).
28. D. Budker, D. Kimball, and D. DeMille, *Atomic Physics: An Exploration through Problems and Solutions* (Oxford University, 2008).
29. B. Patton, E. Zhivun, D. C. Hovde, and D. Budker, "All-optical vector atomic magnetometer," Phys. Rev. Lett. **113**, 013001 (2014).
30. K. L. Corwin, Z.-T. Lu, C. F. Hand, R. J. Epstein, and C. E. Wieman, "Frequency-stabilized diode laser with the Zeeman shift in an atomic vapor," Appl. Opt. **37**(15), 3295–3298 (1998).
31. C. Lee, G. Z. Iwata, E. Corsini, J. M. Higbie, S. Knappe, M. P. Ledbetter, and D. Budker, "Small-sized dichroic atomic vapor laser lock," Rev. Sci. Instrum. **82**(4), 043107 (2011).
32. W. Chalupczak, R. M. Godun, P. Anielski, A. Wojciechowski, S. Pustelny, and W. Gawlik, "Enhancement of optically pumped spin orientation via spin-exchange collisions at low vapor density," Phys. Rev. A **85**, 043402 (2012).
33. D. Budker, W. Gawlik, D. Kimball, S. Rochester, V. Yashchuk, and A. Weis, "Resonant nonlinear magneto-optical effects in atoms," Rev. Mod. Phys. **74**(4), 1153–1201 (2002).

1. Introduction

Light shifts in alkali atoms have been researched since 1960s [1, 2]. The works considering light-shift effects primarily focus either on transitions relevant for atomic clocks [3–8], magnetometers using buffer-gas cells [9–12], or light shifts induced by broad-spectrum alkali-metal lamps [1, 2, 13, 14]. At the same time, the effect of the laser-induced vector light shift (VLS), acting on the magnetic sublevels like a magnetic field, in anti-relaxation coated cells has been little investigated.

In this paper, we discuss the role of VLS in an optical magnetometer exploiting a paraffin-coated alkali-metal vapor cell [15–22]. Unlike uncoated cells, paraffin-coated cells enable the atoms to undergo a number of wall collisions (up to 10^6 [23]) without depolarization. In this way, thermal atoms sample the entire cell volume during their spin relaxation time and hence become sensitive to average, rather than local magnetic field [24]. In this work we demonstrate that the same reasoning can be applied to the VLS in paraffin-coated cells, making it, under realistic assumptions, a function of the total light power averaged over the cell volume, rather than the local light intensity.

The experiment consists of a series of VLS measurements as a function of beam diameter and optical frequency in a synchronously pumped (Bell-Bloom [25, 26]) orientation-based Cs magnetometer. The magnetometer utilizes the resonant response of the atoms to modulated light that occurs when the modulation frequency ω_m matches the atoms' Larmor frequency ω_L. The magnetic field can then be extracted by measuring the center frequency of the Lorentzian shaped magnetic resonance (MR). We investigate the dependence of the light shift, manifesting as a

Optics EXPRESS

frequency change of the MR, on the beam diameter for a fixed optical power and show that with negligible optical pumping the shift is independent of the size of the laser beam (apart from small systematic contributions).

2. Model

To gain understanding of the processes involved in the light-shift averaging, we consider a concentric cylindrical cell and a laser beam with radii R and r, respectively. The optical frequency of the light-shift laser is far-detuned from the relevant atomic transitions compared to the Doppler width, and the beam-intensity profile is for simplicity assumed flat (top hat). In the presence of a magnetic field, the atomic spins precess with the Larmor frequency ω_L. Each individual atom interacting with the light-shift beam acquires a phase advance or retardation ϕ in its Larmor precession proportional to the change in the Larmor frequency due to the vector light shift in the beam $\delta\nu$ and the time t spent in it during the spin coherence time T_2 (T_2 is here the relaxation time for given experimental conditions that is equal to the inverse width of the MR line).

In the proximity of an optical transition, the change in the Larmor frequency by a sufficiently far detuned, circularly polarized laser beam is given by

$$\delta\nu \approx \beta \frac{I}{\Delta_{LS}}, \tag{1}$$

where Δ_{LS} is the frequency detuning of the light-shift (LS) beam with respect to the center of the optical transition (in our experimental setup, this is the center of the Doppler-broadened $F = 4 \rightarrow F' = 3, 4$ transition group of the ^{133}Cs D_1 line), I is the intensity of the LS beam, and β is a proportionality constant that can be calculated with second-order perturbation theory, taking all the relevant transitions and magnetic sub-levels into account (see, for example, [27]).

The scaling of the light-induced MR center frequency shift can be understood as follows: assuming that the probability to find an atom in any part of the cell volume is the same, t is proportional to r^2/R^2, while, when the beam power is kept constant and the beam radius is changed, the beam intensity I scales as $1/r^2$. Since the average phase change acquired by an atom is $\phi \propto I \cdot t$, it does not depend on r. This average phase increment acquired during T_2 can be translated into the average frequency shift of the MR $\delta\nu_{LS}$ by dividing it by the coherence time T_2 of the Larmor precession. Since ϕ is independent of the beam area, $\delta\nu_{LS}$ stays constant for a given light power. Note also that $\delta\nu_{LS}$ is independent of T_2 under the present approximations.

In addition to shifting the MR center frequency, due to the stochastic nature of the interaction of atoms with the light beam, there is also a contribution to the MR linewidth. To estimate this contribution, we consider the different stochastic processes involved and their probability density functions. The number of an atom's transits across the LS beam during a relaxation time follows a Poissonian distribution with mean $n \propto r/R$. At the same time, the amount of phase advance or retardation the atom picks up per pass is normally distributed with mean ϕ_1 and variance $\delta\phi_1^2$. The total shift for the mean number of passes is given by $\phi = n\,\phi_1$ with a variance of $n\,\delta\phi_1^2$. For $\sqrt{n}\,\delta\phi_1 < n\,|\phi_1| \ll 1$ it can be shown [28] that this kind of Larmor precession phase diffusion leads to the previously discussed shift but also to a broadening of the MR. The width increase is due to the uncertainty in the number of interactions per atom as well as the variance $\delta\phi_1^2$ of the LS effect for a single interaction. If the width of the MR stems from a combination of different phase-diffusion processes the contributions add in quadrature.

3. Experimental setup

The foundation of the experimental setup [Fig. 1(a)] is a synchronously pumped Bell-Bloom type magnetometer with an additional laser beam (LS beam) that induces the light shift. The magnetic shielding, the sensor cell, and the leading field $\vec{B}_0$ source are described in [29]. Here, we only

Optics EXPRESS

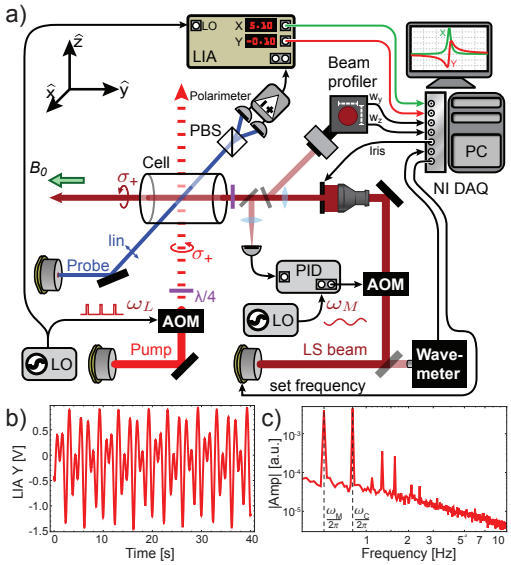

Fig. 1. a) The experimental setup. The amplitude-modulated, circularly polarized pump beam propagates along $\hat{z}$ (orthogonally to $\vec{B}_0 \parallel \hat{y}$). A local oscillator (LO) pulses the pump intensity via an acousto-optical modulator (AOM) and serves as a reference for a lock-in amplifier (LIA), whose analog output is recorded with a data acquisition card (DAQ) and stored on a computer (PC). After transmitting through the cell, the linearly polarized probe beam is analyzed with a balanced polarimeter, consisting of a polarizing beam splitter (PBS) and two photodiodes. The circularly polarized light-shift beam (LS beam) propagates along $\vec{B}_0$. Its diameter is varied with a computer controlled, motorized iris while its time-averaged power is kept constant with an AOM in a feedback loop. An image of the iris is formed inside the cell and on the beam profiler using a lens system. The optical frequency of the LS beam is measured with a wavemeter and controlled by the PC. For noise reduction, we perform synchronous detection of the VLS signal while harmonically modulating the LS beam power at ω_M. b) shows the recorded time series for the LIA Y output for a single light shift measurement with the simultaneous modulation of the LO frequency and the LS power. c) The FFT of the signal in b) shows the calibration peak at $\omega_C/2\pi$ and the LS amplitude at $\omega_M/2\pi$.

recapitulate the main experimental parameters. The paraffin-coated ^{133}Cs cell has a cylindrical shape and measures 50 mm in length and in diameter. Its longitudinal spin relaxation time is 0.7 s. The leading field $\vec{B}_0$ has a magnitude of 489 nT, ($\omega_L = 2\pi \cdot 1710.0$ Hz for the Cs $F = 4$ manifold), and is parallel to $\hat{y}$. The probe light is emitted from a distributed feedback laser (DFB) and tuned to the caesium D_2 line (852 nm) with a power of 9.8 μW. The light is linearly polarized ($\vec{E} \| \hat{y}$) and propagates orthogonally to $\vec{B}_0 \parallel \hat{y}$ (wave vector $\vec{k}_{pr} \parallel \hat{x}$). Its optical frequency is stabilized using a dichroic atomic vapor laser lock [DAVLL [30, 31], not shown in Fig. 1(a)] close to the $F = 4 \rightarrow F' = 3, 4, 5$ transition manifold. The detuning and intensity of the probe beam are optimized for the largest signal with minimal power broadening. The circularly polarized pump light (852 nm DFB, 16.8 μW time averaged) is injected into the cell orthogonally to $\vec{B}_0$ ($\vec{k}_{pmp} \parallel \hat{z}$). Its power is pulsed by an AOM at the Larmor frequency with a 3.4% duty cycle. The beam is routed by a single-mode polarizing fiber (Fibercore HB830Z) with cleanup polarizers at the output. The pump frequency is locked on resonance with the $F = 3 \rightarrow F' = 4$ transition by an additional DAVLL [not shown in Fig. 1(a)]. This produces atomic polarization (orientation) in the $F = 4$ manifold by optically pumping while simultaneously depopulating the $F = 3$ manifold.

Optics EXPRESS

The large detuning from the probed $F = 4$ manifold also minimizes power broadening and light shifts caused by the pump [32]. The LS beam is circularly polarized (895 nm DFB, 5.5 μW time averaged) and propagates parallel to $\vec{B}_0$ so that the vector light shift adds linearly to the Zeeman shift due to $\vec{B}_0$. The beam power is actively stabilized with an AOM in a feedback loop. To change the size of the beam and ensure a homogeneous intensity distribution, the initially Gaussian beam is expanded by a telescope to a large diameter and the central part is picked out by a computer controlled iris with variable aperture. The image of the iris is then formed by a lens system inside the cell and onto a beam profiler (Coherent LaserCam RS-170). For each beam size an image is taken and saved for later analysis. The pick-off for power stabilization and beam profiling is provided by an uncoated wedged beam splitter positioned after the imaging optics outside of the shields just followed by polarizing elements in front of the cell. The optical frequency of the LS beam is actively controlled by a wavemeter (Ångstrom/HighFinesse WS-7) in a feedback loop. The frequency can be set in the computer, where it is compared to the wavemeter measurement. A software feedback controller addresses the laser frequency via an analog output connected to a current modulation input of the laser-diode driver.

As the probe light propagates through the polarized atomic vapor, it experiences magneto-optical rotation [33] which causes a modulation of the probe's polarization direction at the Larmor frequency. The optical signal is detected with a balanced polarimeter connected to a transimpedance amplifier and demodulated with a lock-in amplifier (LIA) at the modulation frequency.

A signal generator (BNC 645) controls the pump pulsing frequency and serves as a local oscillator (LO) for the LIA (SR 830). The phase of the LIA is adjusted to produce absorptive and dispersive signals in the X and Y LIA channels respectively, when the pump-pulse repetition frequency is scanned across the MR. The X and Y signals are captured with a data acquisition system (NI DAQ 6353) and analyzed with a computer (PC) that controls the experiment.

Slow drifts in the the MR center frequency and width pose a challenge for our measurement, as they cause all data points to have a slightly different scaling between the measured signal and the actual light shift. To mitigate this, we simultaneously harmonically modulate the LS beam power and the pump pulsing frequency (in the vicinity of the resonance) at different frequencies. Both signals cause a linear response in the dispersive channel of the lock-in. The latter modulation enables us to continuously monitor the dispersive slope of the MR throughout the experiment since the modulation amplitude is known. We effectively compare the modulation due to the LS beam with a modulation of known amplitude. This way the response of the cell is calibrated for each data point. The modulation frequencies of the LS beam power ($\omega_M = 2\pi \cdot 0.8$ Hz) and the pump pulse frequency ($\omega_C = 2\pi \cdot 0.5$ Hz) are chosen to be smaller than the MR linewidth (3.2 Hz corresponding to $T_2 \approx 100$ ms) to avoid low-pass filtering.

For each data point, we record a 40 s sample of X and Y channels of the LIA. An example can be seen in Fig. 1(b). The signals are Fourier transformed [Fig. 1(c)] and processed to extract the MR linewidth, amplitude and RMS Larmor frequency deviation caused by the LS beam. Each sample has an integer number of periods of both LS and LO modulations to minimize spectral leakage.

4. Results

To see whether the VLS is averaged by the atoms in a paraffin-coated cell, we measure the dependence of the MR center shift as a function of the LS beam area for a given total power (5.5 μW). The average LS intensity is adjusted to keep the total power constant as the beam diameter changes. The smallest beam diameter was given by the maximum available LS beam power and the biggest beam diameter by the minimum value the power could reliably stabilized to with the AOM. The measurement procedure is repeated for different optical frequencies of the LS beam, and each data set is fitted with a linear function. The data and the corresponding fits

Optics EXPRESS

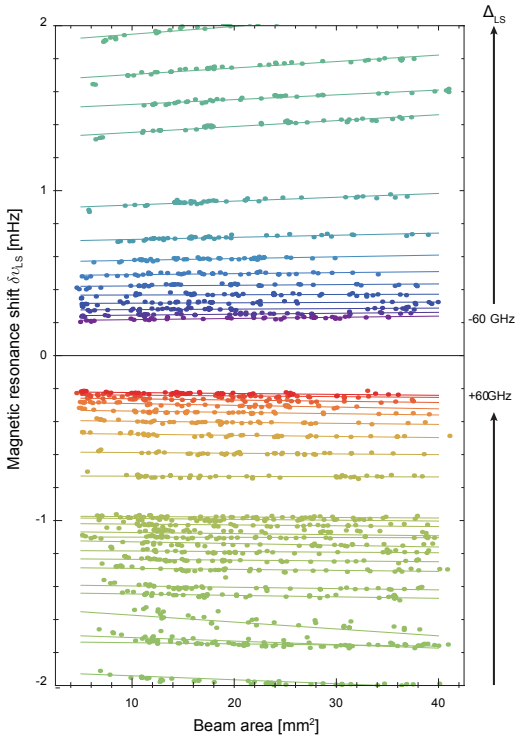

Fig. 2. Change of the magnetic resonance center frequency as a function of the light-shift beam area for different LS beam detunings and a constant beam power. The complete data include detunings from -60 GHz to $+60$ GHz with respect to the ^{133}Cs D_1 $F = 4$ transitions. Just a fraction of the data is displayed here for better visibility of the individual sets. While the beam area x, and therefore the beam intensity, is modified by an order of magnitude, the MR center frequency changes are on average 3% and are of technical origin as explained in the text. Different colors represent distinct optical frequencies of the LS beam, the detuning is indicated by the arrows on the right. The data points are represented by circles, and the lines are linear fits $\delta\nu_{LS}(x) = a_{LS} + b_{LS}(x - \langle x \rangle)$ to the datasets. $\langle x \rangle$ is the mean area of the fitted set. The fit parameters are average light shift a_{LS} and light shift change per unit area change b_{LS}.

are displayed in Fig. 2.

The average light shifts were calculated as an average Larmor frequency change over the data points with different diameters for a given detuning. They are presented in Fig. 3. As shown in Eq. (1), the average light shift scales as $1/\Delta_{LS}$ for large frequency detunings. This dependence is clearly visible in Fig. 3.

The outlier point appearing at $+9$ GHz in Figs. 3 and 4 corresponds to the $F = 3 \rightarrow F' = 3,4$ transitions. This deviation from the theoretical scaling of the VLS (Fig. 3) and the stronger dependence on the beam size (Fig. 4) is a result of optical pumping by the LS beam.

At this frequency, the LS beam acts as an additional pump, producing orientation in the $F = 4$ manifold with effects on the MR width and amplitude. The effect can also be seen at the origin of Fig. 4 corresponding to optical pumping on the $F = 4 \rightarrow F' = 3,4$ transition manifold. Additionally, the absorption in the vapor causes an effective reduction of the LS beam intensity. However, since these are on-resonant effects, a detailed analysis is beyond the scope of this paper.

Optics EXPRESS

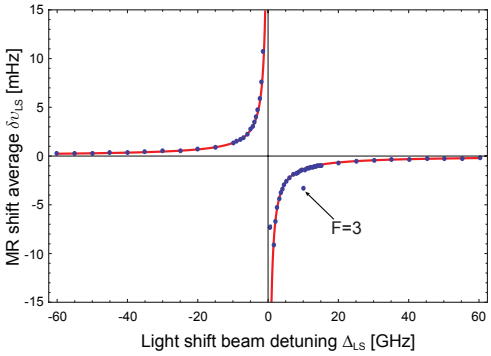

Fig. 3. Average vector light shift a_{LS} dependence on the optical frequency as derived from the fits to the data displayed in Fig. 2. The error bars are hidden within the points since the average ratio between data value and error is 140. The red curve shows a fit to the data with $\propto 1/\Delta_{LS}$.

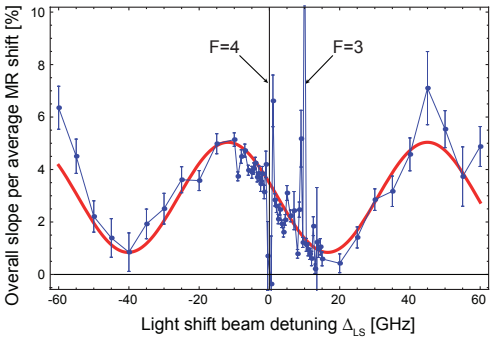

Fig. 4. Light-shift change per unit area b_{LS} divided by the average light-shift a_{LS} (b_{LS}/a_{LS} from Fig. 2) as a function of the LS beam detuning. The data were rescaled to express the change of the measured light shift over each dataset to its mean value in percent. The red line is a sinusoidal fit revealing an etalon effect potentially in the cell wall.

Throughout the experiment the maximum MR center frequency shift was below 100 mHz (30 pT), which is well within the MR resonance width. Signal-to-noise ratio for each data point in Fig. 3 was on average 140 and for large detunings the measurement error was below 1 fT.

The dependence of the VLS on the beam diameter for each optical frequency is presented in Fig. 4. The plot is the result of normalizing the light-shift change per unit area change by the average light shift at each optical frequency (see caption to Fig. 4) A change of the beam area (and therefore of the intensity) by a factor of eight results in an average light shift change on the order of 3%. A likely explanation of this small variation is a systematic effect related to the power stabilization of the LS beam; there seems to be a small diameter dependent difference in power between the cell and the stabilization photodiode. This can have multiple reasons, e.g., clipping of the beam or an angle dependent sensitivity of the photodiode.

In addition to the average change, a sinusoidal variation with the optical frequency detuning is visible. This oscillation pattern appears to be the result of an etaloning effect in the vapor-cell windows. The modulation period of 60 GHz corresponds to a glass-resonator length of 1.7 mm, which is consistent with the thickness of the cell windows. To further verify this, we measured the LS beam power transmission as a function of beam diameter for different LS beam frequencies, which revealed the same pattern.

Optics EXPRESS

In a separate set of similar experiments (not discussed here) we tried to observe the LS-beam-induced broadening of the MR width. Even with much longer averaging no broadening was detected. This is not surprising however, given that the values of $\delta\nu_{LS}$ are much smaller than the MR width. We expect the additional contribution due to $\delta\nu_{LS}$ to be on the order of $\delta\nu_{LS}/\sqrt{n}$, which should be added to the MR width in quadrature (Sec. II). The resulting maximum increase in MR width is less than 10 ppm, which was experimentally inaccessible.

5. Conclusion

In conclusion, we investigated how the vector light shift exerted by a circularly polarized laser beam on atoms in a paraffin-coated cell depends on the beam area. Theoretical estimation suggests that for a given beam power the overall light shift should be independent of the beam area, as long as the thermal atoms adequately sample the entire cell volume during the spin relaxation time. We experimentally verified that the vector light shift in a coated cell depends nearly exclusively on the total beam power and not on the beam area. With a factor of eight change in the beam area, the light shift changes by less than 3%. The residual dependence on the area can be explained by frequency and diameter dependent transmission of the LS beam in the optical elements between the atoms and the intensity-stabilization photodiode. The magnetic resonance broadening due to the variance in the number of passes through the light-shift beam or due to the variance in the time spent in the beam per pass was below the experimental sensitivity. These results are important for modern magnetic sensors that make use of auxiliary fictitious fields [29] and can be extended to other spatially averaged quantities in cells with long coherence times, for example, to the averaging of the scalar and tensor light shifts.

Acknowledgments

We would like to thank Larry R. Hunter for helpful input and comments. This research was supported in part by the National Science Foundation under award CHE-1308381 and by the NGA NURI program. JS and SP would like to acknowledge support from Marie Curie programme, FP7 “Coherent optics sensors for medical applications-COSMA” (PIRSES-GA-2012-295264), and the National Centre for Research and Development within the Leader program.